Simple analytical description of contact pressure and wear evolution in non-conformal contacts

Francesca Di Puccio[1], Lorenza Mattei

Dipartimento di Ingegneria Civile e Industriale, Università di Pisa

Largo Lucio Lazzarino 2, IT56122 Pisa, Italy

francesca.di.puccio@unipi.it, lorenza.mattei@unipi.it

Abstract

The present study proposes an analytical approach to describe contact pressure and wear evolution in line and point contacts. Starting from the unworn condition, described by Hertz theory, modifications of geometry and pressure distribution due to wear are included. Under the basic assumption of parabolic wear and pressure profiles, derived from Finite Element simulations, simple equations governing the phenomenon are derived, where the maximum wear depth evolution is described by a first order differential equation which can be easily solved. Interestingly, the maximum pressure remains dependent on the radius of curvature at the nominal contact point according to Hertz theory, but pressure is not null at the extremes of the contact region. The contact width can be derived from equilibrium conditions and wear law. The reliability of the procedure is proved by the perfect agreement with Finite Element simulations.

Keywords

Wear, wear model, Archard wear law, non-conformal contact, contact pressure, pin-on-plate wear test.

1. Introduction

The evolution of contact pressure and surface geometry as wear occurs is a challenging tribological issue, that has stimulated the interest of many researchers also because of its important consequences in the operational life of mechanical components. Many approaches have been applied to solve this problem, from purely analytical [1,2], to numerical [3–5], some including also lubrication [4,5], surface roughness [6], or with peculiar wear behaviour such as cross-shearing of UHMWPE [7].

Most frequently, the complete description of contact and wear evolution is achieved by means of Finite Element simulations [3,8–11] or boundary element models, e.g. [12,13]. However, they can be rather complex and require a skilled user to correctly set the numerous parameters typically involved in these

[1] Corresponding author

analyses. In a few cases, a combined semi-analytical approach, e.g. [14], or numerical method based on FFT-accelerated procedure were adopted, e.g. [2,15,16]. Purely analytical formulations for estimating wear have been proposed in the past for different tribological pairs, such as for articular joint implants also by the present authors, e.g. [7,17,18].

An exhaustive review of the numerous analytical or semi-analytical models available in the literature is far beyond the aim of this study. Among them, the simplest ones are usually based on geometrical assumptions, i.e. the contact width calculated as the chord of the spherical/cylidrical pin, and/or assume a uniform pressure distribution, as the global incremental wear model (GIWM) in [19]. Also the more complex model developed by Argotov [20], where a the general Hertzian contact is assumed, does not consider the complete evolution of pressure but only its asymptotic trend, when it is almost uniform. Most frequently, the solution requires a discretization both in time and space, with an iterative procedure where pressure can be considered constant within each step . Differently, here we propose a very simple procedure for quantifying wear and contact pressure continuous evolution from the very initial phase to the asymptotic behaviour for non-conformal line/point contacts. In our previous studies, we assumed a constant (unworn) geometry, without updating it due to wear effects and therefore maintaining a constant pressure distribution over time. In this study, a continuous modification of the geometry is considered in a completely analytical formulation, which however moves from fundamental observations of the wear and pressure distributions we obtained from Finite Element simulations [21,22]. As proved in our recent study [23], for the simulated test case, pressure distribution is not affected by friction at least until $f \leq 0.4$. Thus, the present study can be extended also to frictional contacts and can provide rapid and reliable indications to tribologists and engineers.

2. Theoretical Background

Before entering the main equations used in the proposed procedure, its foundations are recalled in the present section.

2.1 Plane curve geometry

Let us consider a planar curve γ in the *x*-*y* plane. It can be described in parametric or explicit form, i.e.

$$\begin{cases} x = x(q) \\ y = y(q) \end{cases} \text{ or } y = y(x)$$

The use of the parametric or explicit form can be chosen to simplify the curve initial equation and wear evolution description. The explicit form is useful when wear can be assumed to occur in the y-direction, as in this case. We will use

$$y_0 = y_0(x) \tag{1}$$

for the new/unworn profile, and

$$y(t,x) = y_0(x) + h(t,x) \tag{2}$$

for the worn curve, depending on time, through the wear depth term $h(t,x)$.

One important feature of the curve for contact pressure description is its curvature $\kappa(t,x)$, or its inverse, the curvature radius $r_c(t,x)$

$$\kappa(t,x) = \frac{y''}{(1+y'^2)^{3/2}} \text{ and } r_c(t,x) = 1/\kappa(t,x) \tag{3}$$

where $y' = \frac{\partial y}{\partial x}$ and $y'' = \frac{\partial^2 y}{\partial x^2}$.

2.2 Wear law

The Archard wear law is frequently used when abrasion and adhesion are the main wear mechanisms involved in the process. It provides a simple relationship between the local wear rate $\dot{h}$ and the contact pressure p

$$\dot{h}(t,x) = k\, v(t,x)\; p(t,x) \tag{4}$$

having denoted with k the wear factor and with v the sliding velocity.

Thus, at a given instant *t,* the linear wear and the loss volume can be obtained by the following integrals

$$h(t,x) = k \int_0^t p(\tau,x)\, v(\tau,x)\, d\tau \tag{5}$$

$$V(t) = \int h(t,x) dA = k \int p(t,x)\, v(t,x)\, dA \tag{6}$$

where *A* is the contact area.

2.3 Hertzian contact equations

As already mentioned, according to [23], pressure distribution is not affected by friction, so in the present study, Hertz solution for non-conformal 2D contacts [24] was used and therefore is briefly recalled in this section. Let us consider two bodies in point contact in *C*, having curvature radii r_1 and r_2 respectively, both made of linear elastic materials, each one characterised by a Young modulus (E_1 and E_2) and a Poisson ratio (ν_1 and ν_2) (Figure 1). We first define the equivalent radius of curvature

$$r_{eq} = \left(\frac{1}{r_1} + \frac{1}{r_2}\right)^{-1} \tag{7}$$

and the equivalent Young modulus

$$E_{eq} = \left(\frac{1-\nu_1^2}{E_1} + \frac{1-\nu_2^2}{E_2}\right)^{-1} \tag{8}$$

The characteristics of pressure distribution differ in case of Line Contact (LC), e.g. cylinder on plane, or Point Contact (PC), e.g. sphere on plane. In the first case, F represents a load per unit length, while it is a force in PC. The maximum contact pressure is related to geometric and material properties as follows

$$p_H^{LC} = \sqrt{\frac{F\,E_{eq}}{\pi\,r_{eq}}}, \qquad p_H^{PC} = \frac{1}{\pi}\sqrt[3]{\frac{6\,F\,E_{eq}^2}{r_{eq}^2}} \tag{9}$$

According to Hertz, the contact pressure is distributed in a small area around the nominal contact point C limited by the contact half-width in LC or radius in PC given by

$$a_H^{LC} = 2\sqrt{\frac{F\,r_{eq}}{\pi\,E_{eq}}}, \qquad a_H^{PC} = \sqrt[3]{\frac{3}{4}\frac{F\,r_{eq}}{E_{eq}}} \tag{10}$$

Both in LC and PC, pressure is maximum at the centre of the contact region and null at the boundary, following a semi-elliptical distribution

$$p(x) = p_H\sqrt{1-\left(\frac{x}{a_H}\right)^2} \tag{11}$$

where x is a radial coordinate in PC.

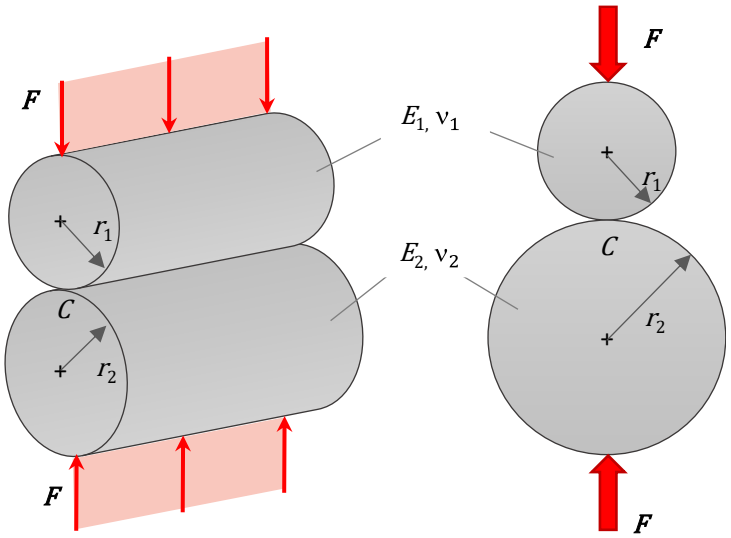

Figure 1 Schemes assumed in Hertz' theory for the cases of (a) line contact between two cylinders and (b) the point contact between two spheres.

3. Material and Methods

3.1 Test cases

As test case for the procedure, the wear evolution in a pin, with head radius r_0 sliding over a plane, with constant velocity v is considered. The cylinder and the plane are assumed to be made of the same material (E and ν), but only the pin is considered to undergo to wear, following the Archard wear law.

This simple scheme was used to describe two different cases (Figure 2):

1) pin-on-plate test where the pin has a cylindrical head, defining a line contact (LC);
2) pin-on disc/plate test where the pin has a spherical head, defining a point contact (PC).

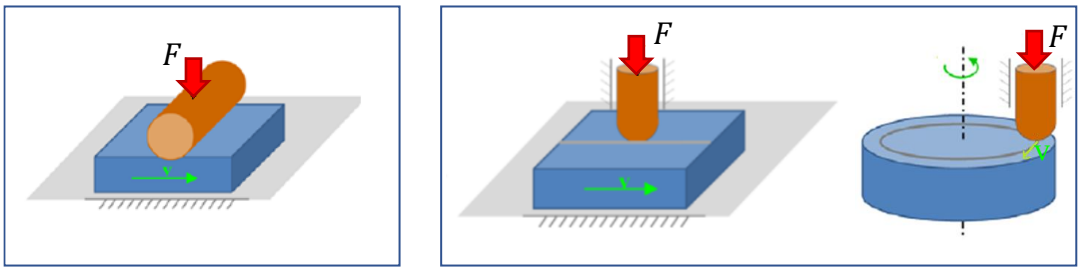

(a) (b)

Figure 2 Schemes of the test cases: (a) line contact: pin-on-plate test, (b) point contact: pin-on-plate/disc test.

For numerical values, we referred to our previous studies already available in the literature, where we used Finite Element (FE) simulations to solve the problems: [21] for LC and [22] for PC. In Table 1, the main data used in the present study are reported, while further details on the FE models can be found in [21,22].

Table 1. Main data for the two numerical test cases.

Test case	r_0 (mm)	E (GPa)	ν	F	k (mm³/N)	v_s (mm/s)	d (mm)
LC [21]	10	200	0.3	100 (N/mm)	10^{-8}	1	1320
PC [22]	5	210	0.3	21 N	$1.25\ 10^{-7}$	25	3000

3.2 Basic equations

3.2.1 Unworn geometry

The general background summarized in Sec.2 can be adapted to the specified test cases, starting from the description of the unworn geometry of the pin (Figure 3).

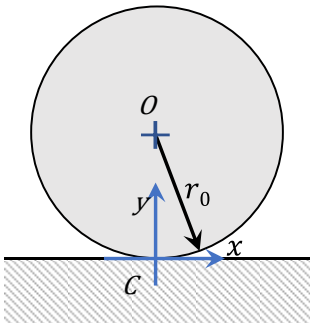

Figure 3 Definition of the geometry in the x-y plane.

In the *x-y* reference system, the lower portion of the circumference containing C is defined by

$$y_0(x) = r_0\left[1 - \sqrt{1 - \left(\frac{x}{r_0}\right)^2}\right] \tag{1.a}$$

3.2.2 Wear distribution

According to Finite Element simulations, the wear profile during wear evolution has always a parabolic distribution, that can be expressed as

$$h(t,x) = \begin{cases} h_M(t)\left[1-\left(\frac{x}{a(t)}\right)^2\right], & |x| \le a(t) \text{ worn portion} \\ 0, & |x| > a(t) \end{cases} \tag{12}$$

This is a fundamental hypothesis as the whole procedure relays on it.

To completely determine the wear profile at a given instant, we need to know $h_M(t)$ and $a(t)$.

The wear volume can be obtained by integrating eq.(12) $h(t,x)$ over time and contact area, that in this case gives simply

$$V(t) = k\, v\, F\, t. \tag{13}$$

3.2.3 Worn profile

Replacing eqs.(1.a) and (12) in eq.(2), the worn profile of the pin becomes

$$y(t,x) = \begin{cases} r_0\left[1-\sqrt{1-\left(\frac{x}{r_0}\right)^2}\right] + h_M(t)\left[1-\left(\frac{x}{a(t)}\right)^2\right], & |x| \le a(t) \\ r_0\left[1-\sqrt{1-\left(\frac{x}{r_0}\right)^2}\right], & |x| > a(t) \end{cases} \tag{14}$$

It should be noted that in eq.(14) wear is considered to occur in the *y*-direction, along the normal to the plane.

3.2.4 Curvature of the worn profile

Since wear modifies the curve profile, the radius of curvature changes with time too. If we focus on the curvature in the nominal contact point C, eq.(3) can be written as

$$\kappa(t,x=0) = \kappa_C(t) = \frac{1}{r_0} + \left.\frac{\partial^2 h}{\partial x^2}\right|_{x=0} = \frac{1}{r_0} - 2\frac{h_M(t)}{a(t)^2} = \frac{1}{r_0}\left(1 - 2\frac{r_0\, h_M(t)}{a(t)^2}\right) \tag{15}$$

$$r_C(t) = \kappa_C(t)^{-1} = r_0\left(1 - 2\frac{r_0\, h_M(t)}{a(t)^2}\right)^{-1} \tag{16}$$

3.2.5 Pressure profile

In the initial condition, the Hertzian solution is adopted, with $r_{eq} = r_0$. Thus, the maximum pressure and the contact half-width in the unworn state, according to eq.(9) and (10) are

$$p_0^{LC} = \sqrt{\frac{F\, E_{eq}}{\pi\, r_0}} \qquad a_0^{LC} = 2\sqrt{\frac{F\, r_0}{\pi\, E_{eq}}} \tag{17}$$

$$p_0^{PC} = \frac{1}{\pi}\sqrt[3]{\frac{6\, F\, E_{eq}^2}{r_0^2}} \qquad a_0^{PC} = \sqrt[3]{\frac{3}{4}\frac{F\, r_0}{E_{eq}}} \tag{18}$$

for line and point contacts. As wear increases, the pressure profile changes rapidly. The distribution observed from Finite Element simulations appears quasi-parabolic, with non-null values at the extremes (Figure 4). Indeed, according to the Archard wear law in eq.(6), pressure is proportional to the linear wear rate, that is,

$$\dot{h}(t,x) = \begin{cases} \dot{h}_M(t) + \left[2\frac{h_M(t)}{a(t)^2}\dot{a}(t) - \dot{h}_M(t)\right]\left(\frac{x}{a(t)}\right)^2, & |x| \le a(t) \\ 0, & |x| > a(t) \end{cases} \tag{19}$$

Thus,

$$p(t,x) = \begin{cases} \frac{1}{k\,v}\left\{\dot{h}_M(t) + \left[2\frac{h_M(t)}{a(t)}\dot{a}(t) - \dot{h}_M(t)\right]\left(\frac{x}{a(t)}\right)^2\right\}, & |x| \le a(t) \\ 0, & |x| > a(t) \end{cases} \tag{20}$$

Since we assumed a uniform sliding velocity in the contact region, at every instant the contact pressure has a parabolic profile (Figure 4) according to the following

$$p(t,x) = \begin{cases} p_M(t) + [p_a(t) - p_M(t)]\left(\frac{x}{a(t)}\right)^2, & |x| \le a(t) \\ 0, & |x| > a(t) \end{cases} \tag{21}$$

where

$$p_M(t) = \frac{\dot{h}_M(t)}{k\,v} \tag{22}$$

$$p_a(t) = p(t, x = \pm a(t)) = \frac{2}{k\,v}\frac{\dot{a}(t)}{a(t)}\,h_M(t) \tag{23}$$

It must be noted that $a(t)$ is the contact half-width but it cannot be obtained from Hertz theory, i.e. eq.(10). On the contrary, the maximum pressure $p_M(t)$ can be estimated by eq.(9), depending on the curvature radius in the nominal contact point as stated by Hertz, i.e.

$$p_M^{PC}(t) = \sqrt{\frac{F\,E_{eq}}{\pi\,r_C(t)}} \qquad p_M^{LC} = \frac{1}{\pi}\sqrt[3]{\frac{6\,F\,E_{eq}^2}{r_C^2(t)}} \tag{24}$$

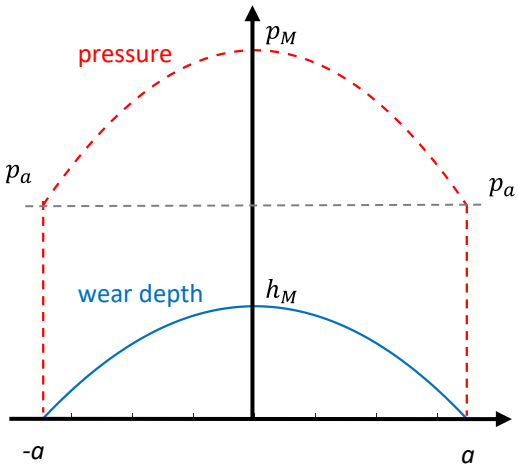

Figure 4 Assumed trends of wear depth and pressure profiles.

3.2.6 Equilibrium equation

At the initial instant, the equilibrium is implicitly guaranteed by Hertz equations. As wear proceeds, the following equilibrium equation should be considered

$$F = \int p(t,x)\, dA$$

For linear contacts, we have

$$F = \int_{-a(t)}^{a(t)} p(t,x)\, dx = \frac{2}{3} a(t)\big(p_a(t) + 2\, p_M(t)\big) \tag{25}$$

that, substituting eqs.(22)-(23) in eq.(25), gives

$$\frac{3}{4} k\, v\, F = \Big(\, \dot{a}(t)\, h_M(t) + \, a(t)\dot{h}_M(t)\Big) = \frac{d}{dt}\big(\, a(t)\, h_M(t)\big)$$

In this specific case where k, v, F are constant, the following equation is obtained

$$\left(\frac{3}{4} k\, v\, F\right)\, t = \, a(t)\, h_M(t) \tag{26}$$

representing an important relationship between the maximum wear depth, the contact half-width and time. The same equation can be obtained from the Archard law. Indeed, taking into account the parabolic wear distribution, the wear volume can be written as

$$V(t) = \int h(t,x) dA = \int_{-a(t)}^{a(t)} h_M(t) \left[1 - \left(\frac{x}{a(t)}\right)^2\right] \mathrm{d}x = \frac{4}{3}\, a(t)\, h_M(t)$$

that, with eq.(13), confirms eq.(26).

For point contacts, due to the axial-symmetry about the y-axis, we have

$$F = 2\pi \int_0^{a(t)} x\, p(t,x)\, dx = \frac{\pi}{2} a^2(t)\big(p_a(t) + \, p_M(t)\big) \tag{27}$$

Also in this case, applying the global Archard equation, another useful relationship can be achieved

$$V(t) = \int h(t,x) dA = 2\pi \int_0^{a(t)} x\, h_M(t) \left[1 - \left(\frac{x}{a(t)}\right)^2\right] \mathrm{d}x = \frac{\pi}{2}\, a^2(t)\, h_M(t)$$

$$\left(\frac{2}{\pi} k\, v\, F\right)\, t = a^2(t)\, h_M(t) \tag{28}$$

3.2.7 Solving equations

a) Line contact

Putting all the things together, inserting eq.(17) in eq.(20), we obtain

$$p_M^{LC}(t) = \sqrt{\frac{F\, E_{eq}}{\pi\, r_C(t)}} = p_0 \, \left(1 - 2\frac{r_0\, h_M(t)}{a(t)^2}\right)^{0.5} \tag{29}$$

and also

$$\dot{h}_M(t) = k\ v\ p_0 \left(1 - 2\frac{r_0\ h_M(t)}{a(t)^2}\right)^{0.5} = \dot{h}_{M0}\ \left(1 - 2\frac{r_0\ h_M(t)}{a(t)^2}\right)^{0.5} \quad (30)$$

Using eq.(26) to calculate $a(t)$

$$a(t) = \left(\frac{3}{4} k\ v\ F\right) \frac{t}{h_M(t)} = c_{FL} \frac{t}{h_M(t)} \quad (31)$$

where

$$c_{FL} = \frac{3}{4} k\ v\ F$$

and inserting it in eq.(30), the solving differential equation can be derived

$$\dot{h}_M(t) = \dot{h}_{M0} \left(1 - 2\ r_0 \frac{h_M(t)^3}{c_{FL}^2\ t^2}\right)^{0.5} \quad (32)$$

b) Point contact

Repeating the above passages for point contact, we have

$$p_M^{PC}(t) = \frac{1}{\pi} \sqrt[3]{\frac{6\ F\ E_{eq}^2}{r_C^2(t)}} = p_0\ \left(1 - 2\frac{r_0\ h_M(t)}{a(t)^2}\right)^{2/3} \quad (33)$$

$$\dot{h}_M(t) = \dot{h}_{M0}\ \left(1 - 2\ r_0 \frac{h_M(t)}{a(t)^2}\right)^{2/3} \quad (34)$$

Using eq.(28) to calculate $a(t)$

$$a(t) = \sqrt{\left(\frac{2}{\pi} k\ v\ F\right) \frac{t}{h_M(t)}} = \sqrt{c_{FP} \frac{t}{h_M(t)}} \quad (35)$$

here

$$c_{FP} = \frac{2}{\pi} k\ v\ F$$

and inserting it in eq.(34), the solving differential equation can be derived

$$\dot{h}_M(t) = \dot{h}_{M0} \left(1 - 2\ r_0 \frac{h_M(t)^2}{c_{FP}\ t}\right)^{2/3} \quad (36)$$

3.2.8 Procedure

Contact and wear evolution are completely determined once $h_M(t)$, $a(t)$, $p_M(t)$ and $p_a(t)$ are known.

As first step, eq.(32) for line contacts or eq.(36) for point contacts must be solved. This can be obtained numerically, e.g. using ode23 solver in Matlab® for $t>0$ or in a discrete form implementing a simple cycle. Once $h_M(t)$ is known, $a(t)$ can be computed by eq.(31) or (35), $p_M(t)$ using eq.(29) or (33), $p_a(t)$ from eq.(25) or (27) for LC or PC, respectively. The whole procedure requires only four simple lines in Matlab®, in addition to input data.

4. Results and discussion

As results of the proposed procedure, in this section we report the obtained trends of the maximum pressure p_M and maximum wear depth h_M during the wear process, versus the travelled distance *d*, both for LC and PC. For validation purposes, analytical results are compared to FE simulations [21,22].

For both LC and PC, the wear of the pin produces a fast decrease of the maximum contact pressure p_M, depicted at the top of Figure 5(a,b), caused by a more and more conformal contact. Accordingly, the maximum wear depth h_M increases non linearly during the running in-phase, whilst almost linearly approaching to the steady state phase, as shown at bottom of Figure 5(c,d).

The increase of contact conformity is well captured by the evolution of contact pressure $p(t,x)$, wear depth $h(t,x)$ and worn profiles $y(t,x)$ at a few selected instants, given in Figure 6, for LC (on the left) and the PC (on the right). In particular, as far as the wear proceeds, the pressure profile flattens, as shown at the top of Figure 6(a,b), and thus the pressure at the centre and the edges of the contact/worn area tends to reach the same value, as well described in Figure 7. Accordingly, the wear depth, always with a parabolic profile, increases in magnitude and width: the curvature radius of the pin increases, the worn profile flattens as plotted at the centre of Figure 6(c, d), thus increasing the contact area.

Since a higher *k* and a longer travelled distance were simulated in the case of PC with respect to LC, the steady state phase of the wear process is shown more clearly for the PC: p_M and p_a assume the same values for a travelled distance higher than about 100 mm (Figure 7), resulting characterized by flat pressure and worn profiles.

The perfect agreement between analytical and FE results both for LC and PC is demonstrated by almost overlapped curves of p_M, h_M, and pressure and worn profiles at given time instants.

The main difference between analytical and FE results consists in the presence of characteristic pressure peaks at the extremes of the worn regions in the FE solution. This is due to a kind of edge effect, with a concentrated loads, generated by the elements at the borders of the worn region, having a discontinuous tangent and curvature of the profile.

The proposed procedure starts with wear, i.e. when *t>0*. Since it is assumed that at the beginning the contact pressure is described by Hertz solution and then becomes parabolic (Fig.6), a 'transition' phase from the elliptic to the parabolic profile should occur. Actually, we did not deepen this transition, because things would not change if we could extend the parabolic trend also for *t=0.* Figure 8 compares for the LC case, the contact pressure profiles in unworn conditions according to the Hertzian theory, the parabolic profile and the FE simulations [21]. They appear very similar, the parabolic profile fits well the contact width estimated by FE simulations, larger that the elliptic hertzian solution. Another difference is the slope of the pressure profile at the borders of the contact, infinite for an Hertzian contact, finite for other two profiles.

With respect to other studies in the literature, e.g. [19,20], in this case a continuous evolution of pressure and wear is obtained with a very simple procedure.

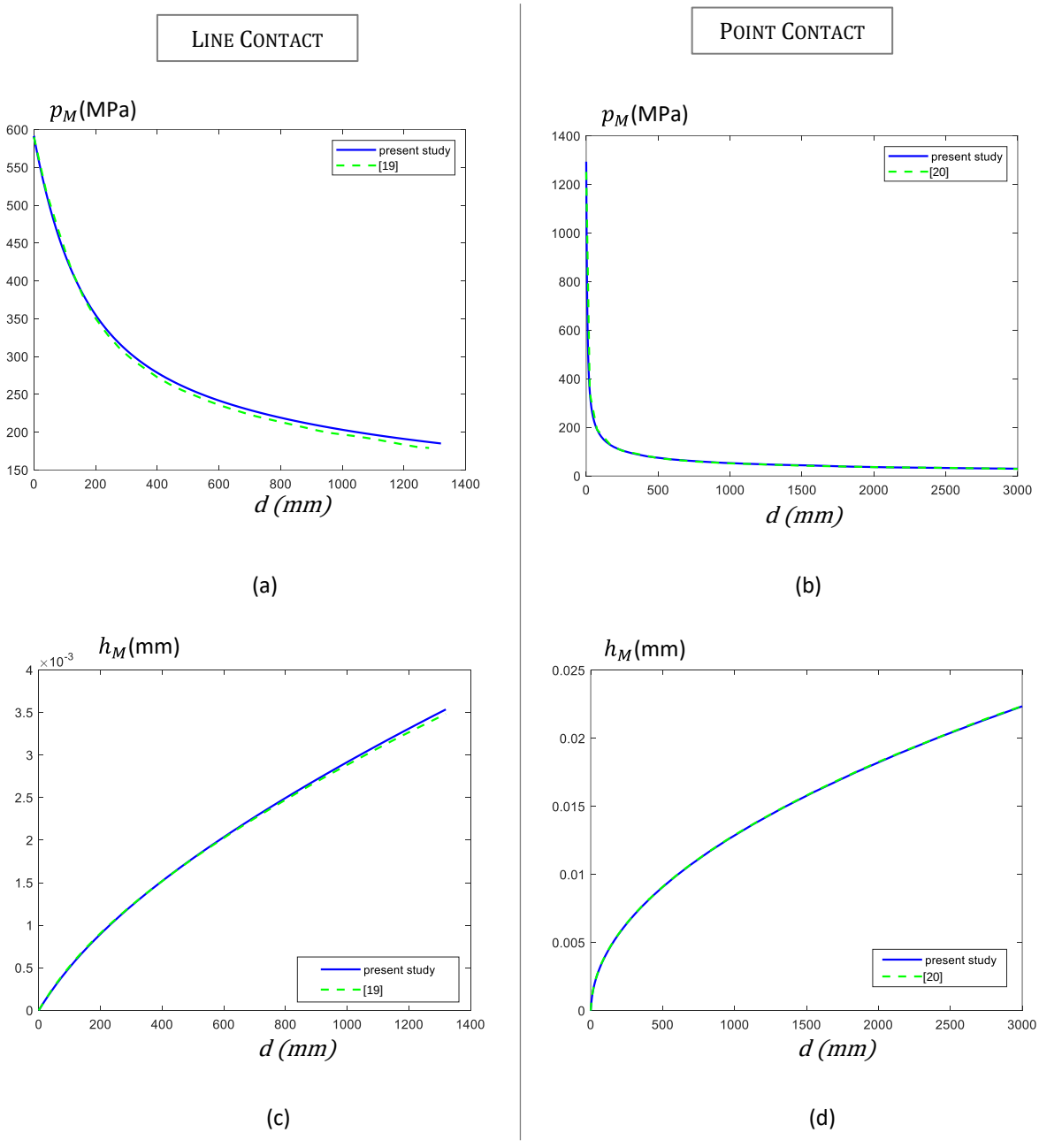

Figure 5 Maximum pressure (top) and wear depth (bottom) history in a line contact (a, c) and ina point contact (b, d): comparison between analytical results and FE simulation([21] for LC and [22] pr PC).

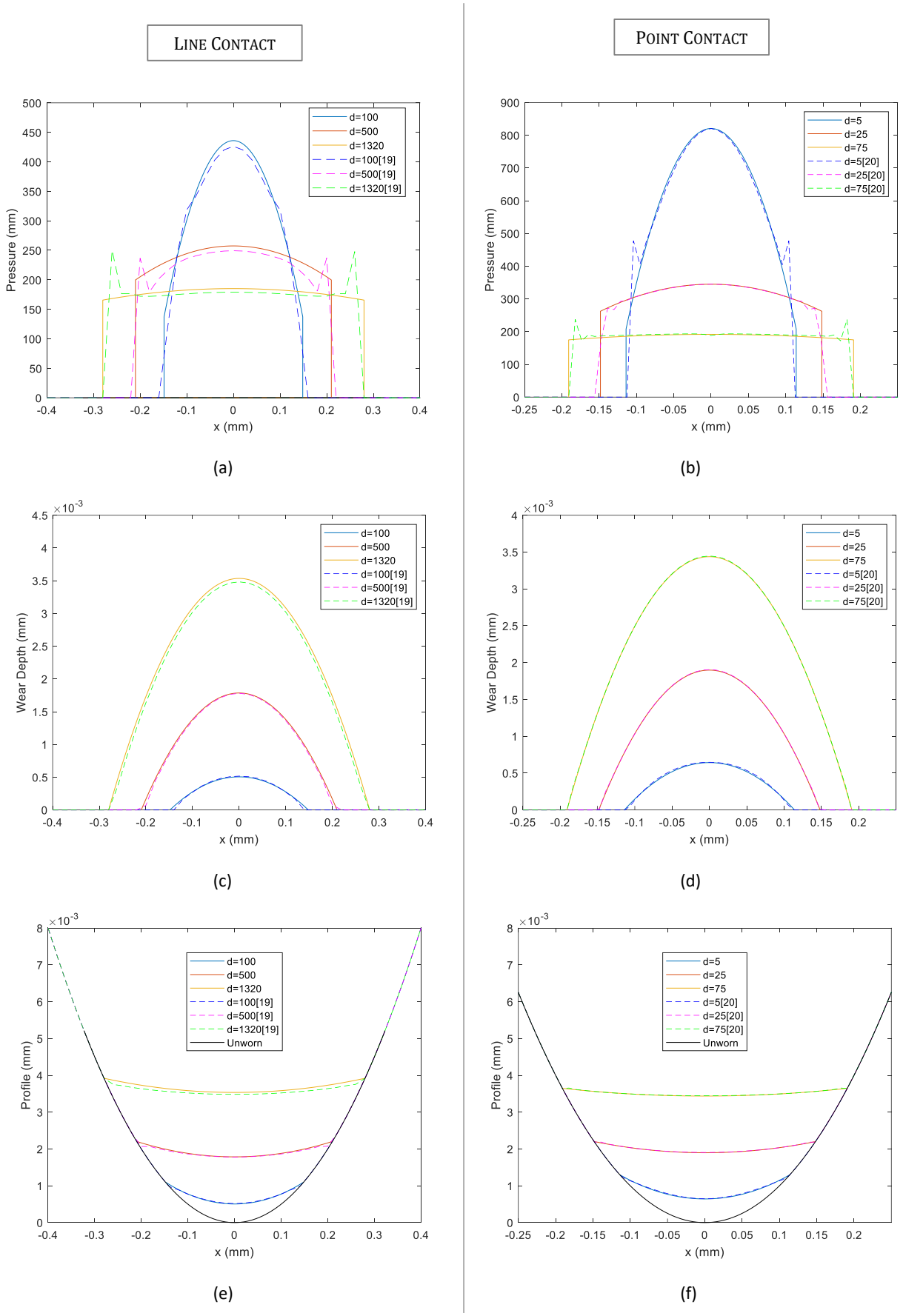

Figure 6 Profiles of contact pressure (top), wear depth (centre) and worn geometry (bottom) at different travelled distances d (mm) for line contact (a, c, e)and point contact (b, d, f): comparison between analytical results and FE simulations ([21] for LC and [22] pr PC).

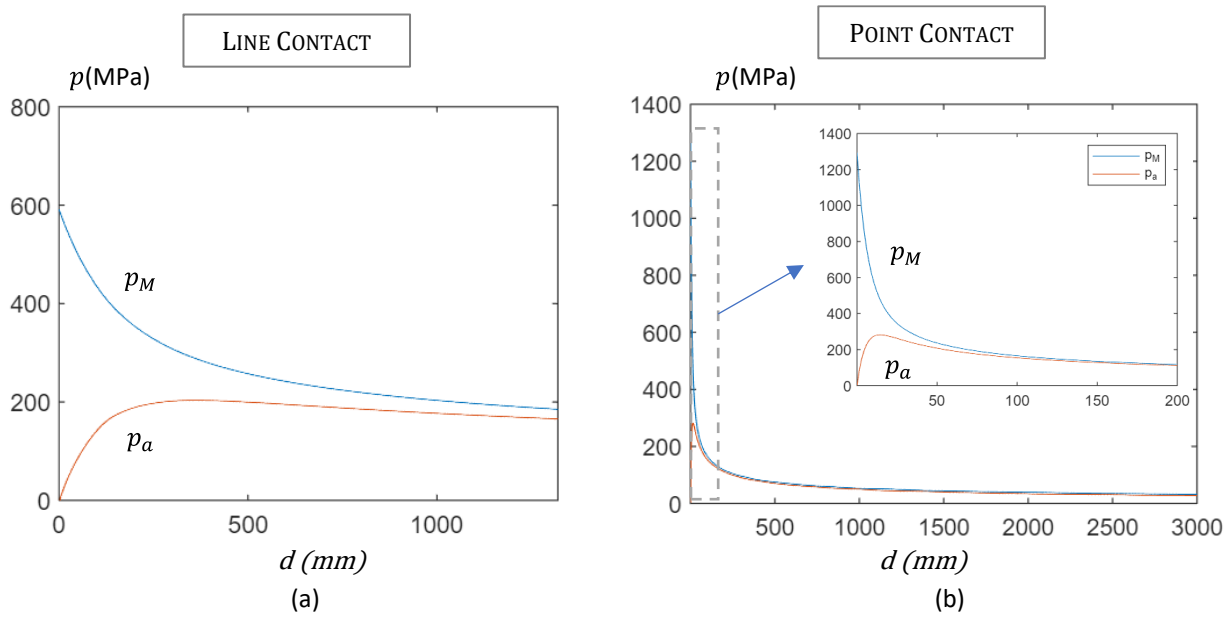

Figure 7 Time history of the maximum contact pressure p_M and the contact pressure p_a at the edge of the worn region for the line contact (a) and the point contact (b).

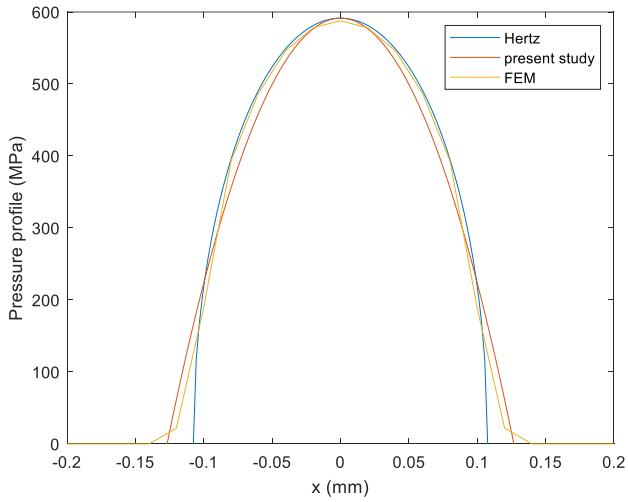

Figure 8 Comparison of the contact pressure profiles in unworn conditions according to Hertzian theory, parabolic profile and FE modelling [21].

5. Conclusions

The present study proposes an analytical approach to describe pressure and wear evolution in line and point contacts. Starting from the unworn condition, described by Hertz theory, modifications of geometry and pressure distribution due to wear are included. The basic assumption, derived from FE studies, is that the wear and pressure profile are parabolic. Under this hypothesis a simple procedure was developed, where the Hertzian formula for estimating the maximum pressure remains valid during the whole wear process. On the other hand, the contact half-width or radius must be estimated by equilibrium condition and Archard wear law. With these simple observations, the evolution of pressure and wear can be easily implemented in few lines of code in Matlab or similar softwaew: the maximum linear wear depth can be calculated by solving a first order differential equation, and then all the other relevant quantities can be easily obtained.

Two numerical test cases were considered to validate the procedure, providing results almost overlapped to Finite Element solutions, thus proving the reliability of the assumption and of the procedure.

One of the major achievements of the proposed analytical approach consists in the simplicity of its implementation and in the extremely low computational cost, few seconds, for the prediction of long term wear. This study can help researchers and engineers to achieve rapid and reliable results on wear and pressure evolution in many practical problems.

6. Bibliography

[1] F. Di Puccio, L. Mattei, In-silico Analytical Wear Predictions: Application to Joint Prostheses, in: Wear Adv. Eng. Appl. Mater., WORLD SCIENTIFIC (EUROPE), 2021: pp. 123–148. https://doi.org/10.1142/9781800610699_0005.

[2] I.I. Argatov, Y.S. Chai, A self-similar model for fretting wear contact with the third body in gross slip, Wear. 466–467 (2021) 203562. https://doi.org/10.1016/j.wear.2020.203562.

[3] L. Mattei, C. Curreli, F. Di Puccio, In-silico Finite Element Wear Predictions, in: Wear Adv. Eng. Appl. Mater., WORLD SCIENTIFIC (EUROPE), 2021: pp. 149–172. https://doi.org/10.1142/9781800610699_0006.

[4] A. Rudnytskyj, R. Larsson, C. Gachot, A Closer Look at the Contact Conditions of a Block-on-Flat Wear Experiment, Lubricants. 10 (2022) 131. https://doi.org/10.3390/lubricants10070131.

[5] Z. Xiao, X. Shi, X. Wang, X. Ma, Y. Han, Lubrication analysis and wear mechanism of heavily loaded herringbone gears with profile modifications in full film and mixed lubrication point contacts, Wear. 477 (2021) 203790. https://doi.org/10.1016/j.wear.2021.203790.

[6] M. Ciavarella, Y. Xu, R.L. Jackson, Some Closed-Form Results for Adhesive Rough Contacts Near Complete Contact on Loading and Unloading in the Johnson, Kendall, and Roberts Regime, J. Tribol. 140 (2018). https://doi.org/10.1115/1.4036915.

[7] L. Mattei, F. Di Puccio, E. Ciulli, A comparative study of wear laws for soft-on-hard hip implants using a mathematical wear model, Tribol. Int. 63 (2013) 66–77. https://doi.org/10.1016/j.triboint.2012.03.002.

[8] E.M. Bortoleto, A.C. Rovani, V. Seriacopi, F.J. Profito, D.C. Zachariadis, I.F. Machado, A. Sinatora, R.M. Souza, Experimental and numerical analysis of dry contact in the pin on disc test, Wear. 301 (2013) 19–26. https://doi.org/10.1016/j.wear.2012.12.005.

[9] P. Põdra, S. Andersson, Simulating sliding wear with finite element method, Tribol. Int. 32 (1999) 71–81. https://doi.org/10.1016/S0301-679X(99)00012-2.

[10] F.J. Martínez, M. Canales, S. Izquierdo, M.A. Jiménez, M.A. Martínez, Finite element implementation and validation of wear modelling in sliding polymer–metal contacts, Wear. 284–285 (2012) 52–64. https://doi.org/10.1016/j.wear.2012.02.003.

[11] C. Mary, S. Fouvry, Numerical prediction of fretting contact durability using energy wear approach: Optimisation of finite-element model, Wear. 263 (2007) 444–450. https://doi.org/10.1016/j.wear.2007.01.116.

[12] G.K. Sfantos, M.H. Aliabadi, A boundary element formulation for three-dimensional sliding wear simulation, Wear. 262 (2007) 672–683. https://doi.org/10.1016/j.wear.2006.08.008.

[13] L. Rodríguez-Tembleque, R. Abascal, M.H. Aliabadi, A boundary elements formulation for 3D fretting-wear problems, Eng. Anal. Bound. Elem. 35 (2011) 935–943. https://doi.org/10.1016/j.enganabound.2011.03.002.

[14] J. Lengiewicz, Efficient model of evolution of wear in quasi-steady-state sliding contacts, (2013) 11.

[15] J. Andersson, A. Almqvist, R. Larsson, Numerical simulation of a wear experiment, Wear. 271 (2011) 2947–2952. https://doi.org/10.1016/j.wear.2011.06.018.

[16] I.I. Argatov, Y.S. Chai, Artificial neural network modeling of sliding wear, Proc. Inst. Mech. Eng. Part J J. Eng. Tribol. 235 (2021) 748–757. https://doi.org/10.1177/1350650120925582.

[17] L. Mattei, F. Di Puccio, Wear Simulation of Metal-on-Metal Hip Replacements With Frictional Contact, J. Tribol. 135 (2013) 021402. https://doi.org/10.1115/1.4023207.
[18] L. Mattei, F. Di Puccio, T.J. Joyce, E. Ciulli, Effect of size and dimensional tolerance of reverse total shoulder arthroplasty on wear: An in-silico study, J. Mech. Behav. Biomed. Mater. 61 (2016) 455–463. https://doi.org/10.1016/j.jmbbm.2016.03.033.
[19] V. Hegadekatte, S. Kurzenhäuser, N. Huber, O. Kraft, A predictive modeling scheme for wear in tribometers, Tribol. Int. 41 (2008) 1020–1031. https://doi.org/10.1016/j.triboint.2008.02.020.
[20] I.I. Argatov, Asymptotic modeling of reciprocating sliding wear with application to local interwire contact, Wear. 271 (2011) 1147–1155. https://doi.org/10.1016/j.wear.2011.05.028.
[21] L. Mattei, F. Di Puccio, Influence of the wear partition factor on wear evolution modelling of sliding surfaces, Int. J. Mech. Sci. 99 (2015) 72–88. https://doi.org/10.1016/j.ijmecsci.2015.03.022.
[22] C. Curreli, F. Di Puccio, L. Mattei, Application of the finite element submodeling technique in a single point contact and wear problem, Int. J. Numer. Methods Eng. 116 (2018) 708–722. https://doi.org/10.1002/nme.5940.
[23] L. Mattei, F. Di Puccio, Frictionless vs. frictional contact in numerical wear predictions of conformal and non-conformal sliding couplings (Accepted for publication), Tribol. Lett. (2022).
[24] H. Hertz, Über die berührung fester elastische körper J Für Die Reine U Angew Math, 92 (1882), pp. 156-171, (1882) 156–171.